Sensors and Actuators B 156 (2011) 147–155

Contents lists available at ScienceDirect

Sensors and Actuators B: Chemical

journal homepage: www.elsevier.com/locate/snb

Electrical and CO gas sensing properties of nanostructured $La_{1-x}Ce_xCoO_3$ perovskite prepared by activated reactive synthesis

Mohammad Ghasdi[a], Houshang Alamdari[a,*], Sébastien Royer[b], Alain Adnot[a]

[a] Department of Mining, Metallurgical and Materials Engineering, Université Laval, Québec G1V 0A6, Canada
[b] Université de Poitiers, LACCO - UMR 6503 CNRS, 40 Avenue du Recteur Pineau, 86360 Poitiers, France

ARTICLE INFO

Article history:
Received 6 January 2011
Received in revised form 25 February 2011
Accepted 2 April 2011
Available online 13 April 2011

Keywords:
Perovskite
Nanostructured
CO sensor
Cerium
High energy ball milling
$LaCoO_3$

ABSTRACT

A series of nanostructred $La_{1-x}Ce_xCoO_3$ perovskite-type (x ranging from 0 to 0.2), with a crystallite size of around 10 nm and a specific surface area of up to 55 m^2/g were prepared using the activated reactive grinding method. XRD results showed that Ce segregates as CeO_2 when the addition level exceeds 10 at%. CO was chosen as a typical reducing gas and its interaction with surface oxygen was investigated. TPD-O_2 was used to investigate the effect of Ce-doping on total surface oxygen. The experimental results confirmed a positive effect of Ce-doping of up to 10 at% on total surface oxygen (α-O_2). TPD-CO and XPS analyses were performed to find the total carbon adsorption (i.e. related to the adsorption of CO) on the surface of the synthesized samples. Both methods confirmed that more carbon adsorbs on the surface of doped formulations compared to the pure $LaCoO_3$. Ce-doping increases the surface oxygen, thereby facilitating the adsorption and oxidation processes. CO gas sensing properties of thick $La_{1-x}Ce_xCoO_3$ films were performed. $La_{0.9}Ce_{0.1}CoO_3$ showed the highest conductivity and the lowest activation energy. The optimum CO sensing temperature for doped formulation was found to be 100 °C compared to 130 °C for pure perovskite. Ce-doped samples showed a maximum response ratio of 240% with respect to 100 ppm CO in air compared to 60% obtained with pure $LaCoO_3$.

1. Introduction

Recently, a number of mixed-metal oxides with a perovskite-type structure and the overall formulation of ABO_3 have received considerable attentions as catalyst and gas sensor materials because of their thermal and chemical stability [1–4]. The activity of perovskites is practically determined by the nature of their cations, which play an important role in adsorption of gas species and their catalytic activities. The electronic properties and catalytic activity of the perovskite-type oxides can be modified by substitution of ions into the A or B sites [5].

Most of the published reports on gas sensing properties of perovskites have been reviewed by Fergus [6]. As a CO gas sensor, a variety of undoped perovskites including titanates [7], ferrites [8], cobaltates [9] and doped formulations [9–11] have been reported. Partial substation of A or B site cations in some cases resulted in a positive effect on the gas sensing performance. For example, in $LaFeO_3$ system substitution of Pb on the La site [12] and/or of Co on the Fe site [13] increased the sensing performance while substitution of Sr on the La site [14] or of Mg on the Fe site [14] did not result in a significant improvement in gas sensing properties. On the other hand, the response of $LaCoO_3$ to CO was improved by doping Sr on the La site and Cu or Ni on the Co site [15].

Cerium doping (up to 10 at%) on the A site in cobalt or manganese-based perovskites usually leads to an increase in oxidation catalytic activity [16–21]. Oxidation of CO on perovskite-type materials is a superficial reaction where the gas species react with the surface oxygen. The availability of more oxygen on the surface may result in higher catalytic activity. The consequences of partial substitution of Ce(IV) on the La(III) site are the reduction of a fraction of Co(III) to Co(II) and/or a change in oxygen stoichiometry to ensure the charge compensation. Oxygen can be adsorbed and reduced on the Co(II) sites to produce Co(III)/O'_2 species [34] An increase in the Ce doping on the structure is expected to increase the number of surface oxygen, thus facilitating the oxidation reaction. However, the solubility limitation of Ce doping on the $La_{1-x}Ce_xCoO_3$ structure results in a saturation point in the structure. More Ce doping after the saturation point may increase the level of impurities and decrease the overall activity.

In addition to the chemical composition, the structural features of perovskite materials have a significant influence on their

* Corresponding author. Tel.: +1 418 656 7666; fax: +1 418 656 5343.
E-mail address: Houshang.alamdari@gmn.ulaval.ca (H. Alamdari).

0925-4005/$ – see front matter © 2011 Elsevier B.V. All rights reserved.
doi:10.1016/j.snb.2011.04.003

response with respect to gas species. Nanostructured metal oxides with a higher surface area and a smaller crystallite size offer the potential for a substantial increase in the performance of gas sensors as compared to that offered by conventional microcrystalline materials [22]. In the synthesis of nanocrystaline perovskite oxides, a number of techniques have been used to reduce particle size to the extent possible [23–25]. However, in order to form a perovskite structure and to remove the organic precursors, high calcination temperatures (typically above 600 °C) are usually required. A high calcination temperature enhances solid-state diffusion, reducing the specific surface area and increasing the mean crystallite size which grows with calcinations temperature and time. Some researchers have reduced the calcination temperature to reach higher SSA and lower particle size by using complex or expensive methods. For example, spray-freezing/freeze-drying [26] and Schiff base complex sol–gel [27] have been used to prepare $LaCoO_3$ with an average crystallite size of 20 nm and SSAs of 24 and 11.7–18.6 m^2/g, respectively, with the calcinations temperature kept as low as 500 °C. Both traditional and new methods of synthesis of nanostructured perovskites have considerable manufacturing issues basically due to low production rates, high costs, and expensive waste treatment.

Activated reactive synthesis is an alternative method to synthesize nanocrystalline metal oxide at quasi room temperature [28,29]. This method is essentially a combination of high energy and low energy ball milling steps. The former reduces the particle size while the latter enhances deagglomeration and increases the specific surface area. A wide variety of perovskites including simple perovskites and the doped ones with a crystallite size down to 10 nm and a SSA up to 100 m^2/g have been synthesized by this technique [29,30]. Royer et al. [31] showed the effect of high energy ball milling (HEBM) on bulk and grain boundary of perovskite oxides and their relation with oxidation reaction. HEBM creates nanostructured materials with a high density of grain boundaries, which can accelerate the diffusion of oxygen. Perovskites with a higher theoretical specific surface area have shown a higher grain boundary volume and subsequently a higher oxygen mobility and catalytic activity [31]. In our previous work [32], we used the activated reactive grinding method to synthesize nanostructured $LaCoO_3$ perovskite, which resulted in a surface area of 70 m^2/g and a small crystallite size (10 nm) accompanied by an improved CO sensing performance. $LaCoO_3$ synthesized using this method showed a better CO gas sensing behavior (lower temperature and higher sensitivity) as compared to the samples prepared using other methods such as the sol–gel and the solid-state reaction. The improved sensing performance was attributed to the higher oxygen mobility of the sensor.

In the study reported here, the effect of cerium doping on gas sensing behavior of $La_{1-x}Ce_xCoO_3$ prepared by activated reactive grinding method was investigated. The aim was to exploit the effects of both structural features and chemical composition in order to increase the oxygen mobility and consequently the gas sensing performance of LaCo-based perovskites. Five formulations with nominal compositions of $La_{1-x}Ce_xCoO_3$ (x = 0–0.2) were prepared. The principal objective of the study was therefore to provide new information on the mechanism through which the sensing properties of LaCo-based perovskite are influenced with respect to a typical reducing gas. CO was chosen as a typical reducing gas and its interaction with sensing material was investigated. Physicochemical characteristics of the sensing material were used to interpret the influence of Ce-doping on the samples' sensing behavior with respect to CO. Although the selectivity aspect was not addressed in this study, the behavior of the material under other reducing gas species was expected to follow the same trend, except for the maximum response temperature and amplitude.

2. Experimental details

$La_{1-x}Ce_xCoO_3$ (x = 0, 0.05, 0.1, 0.15, 0.2) nanostructured perovskites, labelled as Cex (x = mol fraction of doping in La-site), were prepared by the activated reactive synthesis method. La_2O_3, CeO_2 and Co_3O_4 with a purity of 99.8% were dehydrated at 550 °C to remove any hydrate from the oxides. They were subsequently weighed at the required molar ratio for each formulation and mixed together. This was followed by a heat treatment at 1000 °C for 2 h. Five grams of pre-mixed materials were introduced into a tungsten carbide (WC) crucible containing WC balls, and milled for 2 h. In order to deagglomerate the synthesized material, a second milling step was performed with a lower milling energy for 1 h. In this step, a laboratory attritor containing 4.5-mm hardened steel balls was used. Both milling times were the optimized times as reported earlier [32].

Powder X-ray diffraction (XRD) patterns were recorded using a diffractometer (SIEMENS D5000) with Cu/Kα radiation (λ = 0.154 nm) and a 0.05° step scan from 15° to 80° in 2θ angles. The average crystallite size (D) was calculated by means of the Debye–Scherrer equation $D = K\lambda/(\beta \cos\theta)$ after doing the Warner's correction for instrumental broadening. Phase identification was performed using the JCPDS data bank.

BET specific surface area of the powders was determined by adsorption/desorption isotherms of N_2 at −196 °C using ChemBET Pulsar TPR/TPD/BET (Quantachrome). Before each BET test, the powders were degassed at 200 °C for 6 h under helium. Temperature programmed desorption of oxygen (TPD-O_2) was performed using the same equipment. A hundred and fifty mg of powder was placed in a quartz cell and calcined at 200 °C for 6 h. The sample was then pre-treated at a flow of 5% O_2 in He (20 ml/min) at 300 °C for 2 h, followed by cooling down to room temperature at the same flow. The gas flow was switched to pure He with a flow rate of 100 ml/min and the TPD-O_2 was carried by increasing the temperature. The temperature was increased from 25 to 900 °C with a heating rate of 5 °C/min, and kept at 900 °C for 15 min to obtain the complete desorption process. Desorption of oxygen was monitored and quantified using a thermal conductivity detector (TCD).

To obtain a thick sensing film on alumina rod substrates, the wash coating method was used. Ten percent of the perovskite powder was dispersed in DI water using an ultrasonic bath. The pH of the slurry was adjusted at 3. This pH value, one that allowed for a smooth and even coating, was achieved through trial and error. Some drops of prepared slurry were instilled on the alumina rod substrate (25.4 mm in length and 4.7 mm in diameter). Coated samples were dried overnight at room temperature and annealed at 400 °C for 2 h with a heating and a cooling rate of 10 °C/min. Metallic electrodes were then connected to the coated samples for gas testing.

CO gas testing was performed in a homemade system consisting of a stainless chamber with a capacity of 800 ml in which three samples can be hung up via a high temperature feed-through. This chamber was placed in the adjustable and programmable furnace with a precision better than 1 °C. The temperature of the chamber was monitored with a K-type thermocouple, which was placed close to the samples surface. A gas mixing system with a precision of 0.2% of the full scale provided the required CO concentration and flow rate. The gas flow was entering the chamber at the bottom and was exiting it from the top. For this experiment, resistance variations were recorded as a function of time, temperature and gas compositions. All resistances, temperature, gas flow and concentration were recorded every second using an Agilent 34970A data acquisition unit. For each gas testing procedure, coated samples were heated up to 350 °C under dry air to remove any adsorbed gases and humidity from the sensing film. They were then cooled down to, and maintained at, the desired temperature to stabilize the

resistance. A mixture of CO and dry air was then introduced into the chamber for 30 min with a flow rate of 100 ml/min. This procedure was repeated four times to compare the obtained results and to verify the repeatability of the response. The response ratio at the constant temperature was calculated using the following equation:

$$\text{Response ratio} = \frac{(R_{gas} - R_{air})}{R_{air}} \times 100$$

where R_{gas} is the resistance at a given temperature and under a given CO concentration, and R_{air} is the base resistance at the same temperature under dry air.

Temperature programmed desorption of carbon monoxide (TPD-CO) was performed by means of the same equipment as used for TPD-O_2. A hundred and fifty mg of powder was degassed and oxidized under the same conditions as those of the TPD-O_2, which was then exposed to 100 ppm CO in dry air at 100 °C for 1 h. The sample was subsequently cooled down to room temperature under the same gas flow. The desorption process was performed under helium with a heating rate of 5 °C/min. CO and CO_2 concentrations were monitored using an FTIR gas analyzer (ABB EL3020 CO, CO_2 analyser).

An analysis of the samples' surface composition was run using an X-ray photoelectron spectroscopy (XPS) using a mono-chromatized Al Kα X-ray radiation source at 20 mA and 15 kV. To reveal the effect of gas on the surface oxidation state, a variety of treatments were performed. First, in order to eliminate the surface contamination due to any carbonate groups, the samples were kept under pure air flow at 100 °C for 10 h. The samples were then heated to 300 °C, maintained at this temperature for 2 h and cooled down to room temperature. These treatments simulated the pre-treatments applied prior to any gas sensing tests. XPS analyses were performed to reveal the surface state of the samples, that is their state before injecting the target gas. In the second step, after degreening at 300 °C under pure air, the samples were cooled down to 100 °C. This was followed by injecting100 ppm CO into the flow gas for 1 h. The treated samples were then passed onto the XPS's testing chamber to undergo surface analyses for the investigation of the effects of their exposure to CO.

3. Results and discussion

The X-ray diffraction patterns of Ce-doped $La_xCe_{1-x}CoO_3$ (x = 0, 0.05, 0.1, 0.15, 0.2) powders are shown in Fig. 1. The XRD patterns confirmed the perovskite structure of the synthesized material. A small quantity of unreacted CeO_2 appeared in all doped formulations while the intensity of CeO_2 peak rose when increasing the Ce doping level. In general, a perovskite structure is formed when the tolerance factor is in the range of 0.8–1 [5]. The tolerance factor "t", is influenced by the ionic radius of the perovskite's constituents as expressed by the following equation:

$$t = \frac{r_A + r_B}{\sqrt{2}(r_B + r_O)}$$

where r_A and r_B are the ionic radii of the cations in A and B sites respectively, and r_O is the ionic radius of oxygen. Replacing La^{3+} with Ce^{4+} of a lower cation radius would decrease the tolerance factor, resulting in the aberration of the perovskite structure. This could, moreover, influence the tolerance factor by changing the radius of Co ions. In essence, the consequence of partially replacing La^{3+} with Ce^{4+} of a higher oxidation state results in either a partial transformation of Co^{3+} to Co^{2+} or in a change in the oxygen stoichiometry. This is because the electrical neutrality of the crystal should be maintained. The ionic radius of Co^{2+} is larger than that of Co^{3+}, which could in turn decrease the tolerance factor. By replacing La with Ce, the tolerance factor will decrease as far as its lower limit at which point the A-site is considered saturated as no more substitution would be possible. Further Ce addition may, therefore, result in the segregation of Ce-oxide impurities. The saturation point for Ce-doping has been variously reported in other studies to be between 5 and 10 at% [33,34].

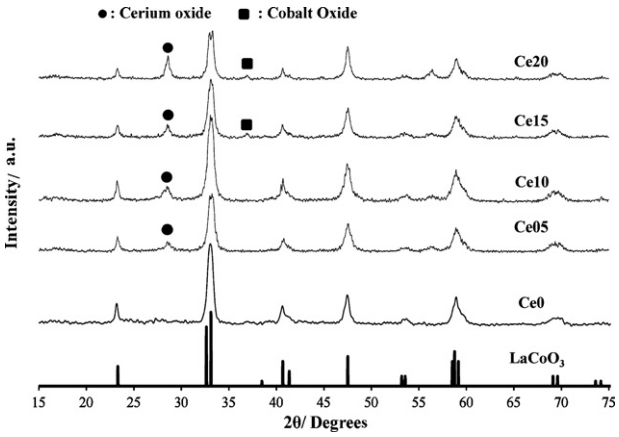

Fig. 1. XRD-patterns of $La_{1-x}Ce_xCoO_3$ (x = 0, 0.05, 0.1, 0.15 and 0.2) synthesized powders.

The XRD patterns reveal that a small amount of cobalt oxide also appears in the synthesized material when the addition level of Ce exceeds 10 at%. This phenomenon is related to the decrease of the La/Co atomic ratio as well as to the fact that extra CeO_2 cannot react with the Co_3O_4 to form a perovskite structure. Since Ce is added to the formulation at the expense of La, increasing the quantity of the unreacted CeO_2, would decrease the La level, leading to a lack of the La necessary for the formation of a perovskite structure. Thus, a further increase in the unreacted CeO_2 will also cause the formation of Co-oxide impurities.

Table 1 summarizes the mean crystallite size, as calculated with the Debby-Scherer equation, as well as the specific surface area of all samples both after the first milling step and following the activation step (the second milling step). The mean crystallite size of all the doped samples is around 10 nm, falling in the same range as that of the pure $LaCoO_3$. This confirms that the HEBM is capable of producing the same crystallite size for different Ce addition levels. N_2 adsorption/desorption measurements for the samples after the first milling step showed that the BET specific surface area of all samples was in the same range (typically less than 4 m^2/g). The activation process managed to increase the surface area to

Table 1
Specific surface area, crystallite size and synthesized phases.

Sample	Target composition	Crystalline phase	Mean crystallite size (nm)	SSA (m^2/g) milling step	SSA (m^2/g) activation step
Ce0	$LaCoO_3$	P	11	3.8	66
Ce05	$La_{0.95}Ce_{0.05}CoO_3$	P, Ce	12	3.5	54
Ce10	$La_{0.9}Ce_{0.1}CoO_3$	P, Ce	12	3.6	56
Ce15	$La_{0.85}Ce_{0.15}CoO_3$	P, Ce, Co	13	3.4	52
Ce20	$La_{0.8}Ce_{0.2}CoO_3$	P, Ce, Co	13	3.3	50

P: perovskite, Ce: cerium oxide, Co: cobalt oxide.

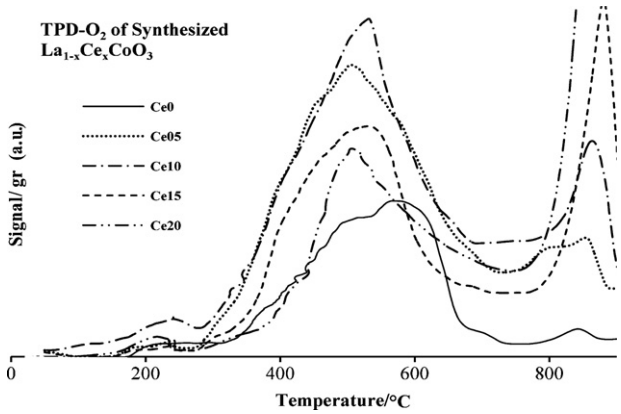

Fig. 2. TPD-O_2 of $La_{1-x}Ce_xCoO_3$ (x = 0, 0.05, 0.1, 0.15 and 0.2) synthesized powders.

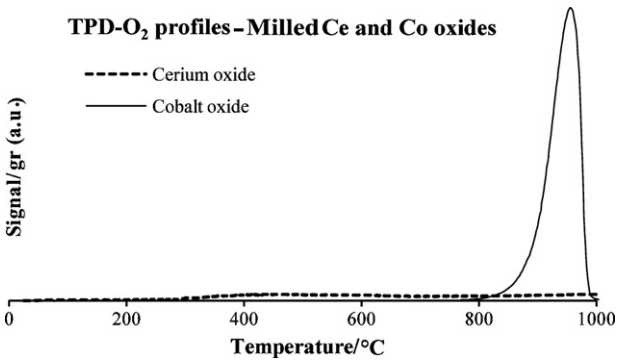

Fig. 3. TPD-O_2 of pure and milled CeO_2 and Co_3O_4 oxides.

around 50–55 m^2/g. This is slightly lower than that obtained for pure $LaCoO_3$ samples. The difference could be accounted for by the agglomeration state of the unreacted precursors of CeO_2 and Co_3O_4. We have already reported the efficiency of the activation process in increasing the specific surface area of $LaCoO_3$ perovskite samples, and have demonstrated the effect of the process on the oxygen desorption and sensing properties of these materials [32].

Fig. 2 shows the normalized TPD-O_2 results of the synthesized powders with different Ce addition levels. Two types of oxygen have usually been reported in the literature. The first, denoted as α-O_2, is desorbed from the surface of the solid, and the second one, denoted as β-O_2, is desorbed from the bulk. α-O_2 desorbs at temperatures lower than 700 °C, with its quantity being approximately equal to one monolayer of adsorbed oxygen on the available surface area [10]. However, researchers have shown highly agglomerated nanocrystalline perovskite with a large number of grain boundaries to be capable of desorbing more than one monolayer oxygen [31]. This extra oxygen comes from the grain boundaries, which act as an extra source of oxygen. In our previous work, we reported that high diffusion rates in grain boundaries compared to that of the grain interior would make them a source of early oxygen desorption [32].

Comparing the TPD-O_2 results clearly reveals the effect of Ce doping on α-O_2 desorption. The maximum desorption tempera-

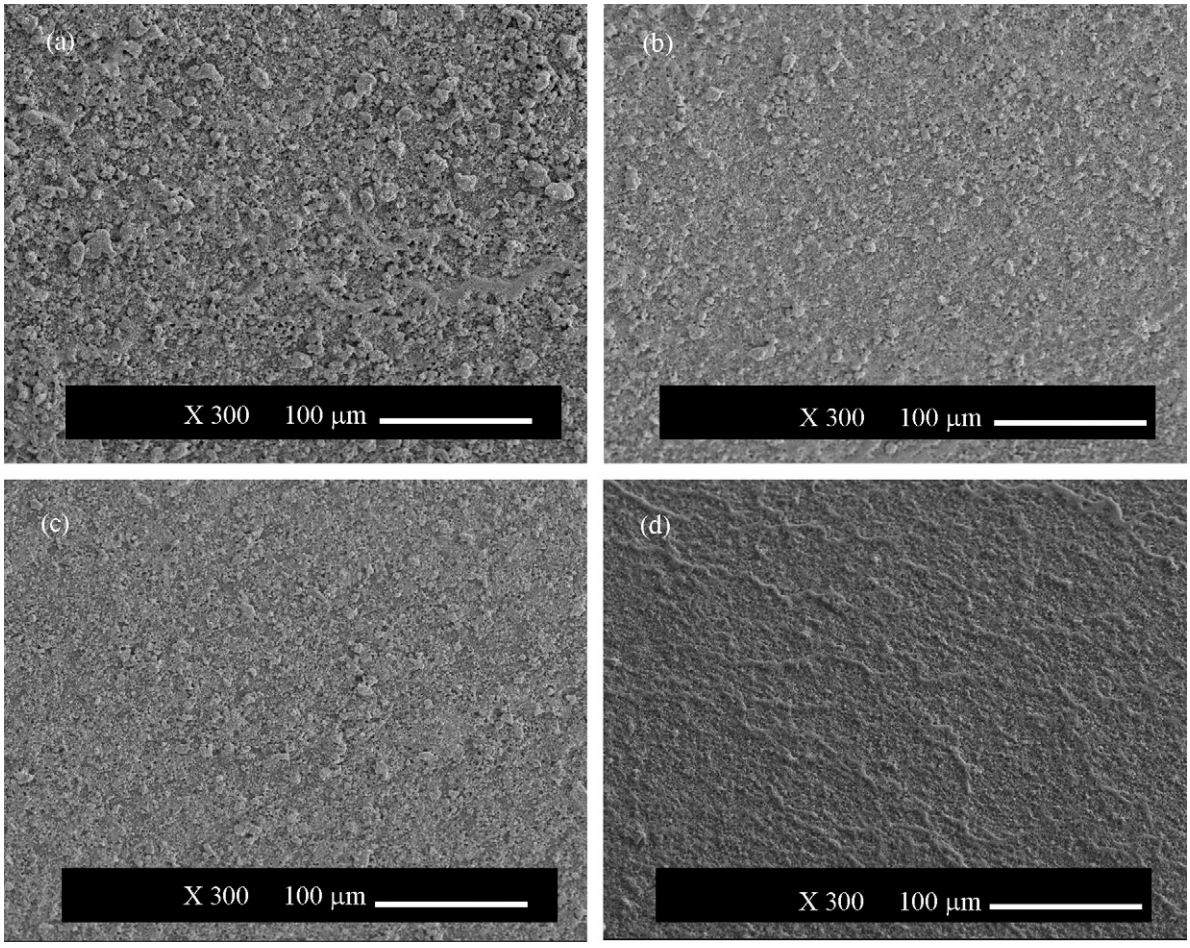

Fig. 4. SEM images of coated samples: (a) $La_{0.95}Ce_{0.05}CoO_3$, (b) $La_{0.9}Ce_{0.1}CoO_3$, (c) $La_{0.85}Ce_{0.15}CoO_3$ and (d) $La_{0.80}Ce_{0.2}CoO_3$.

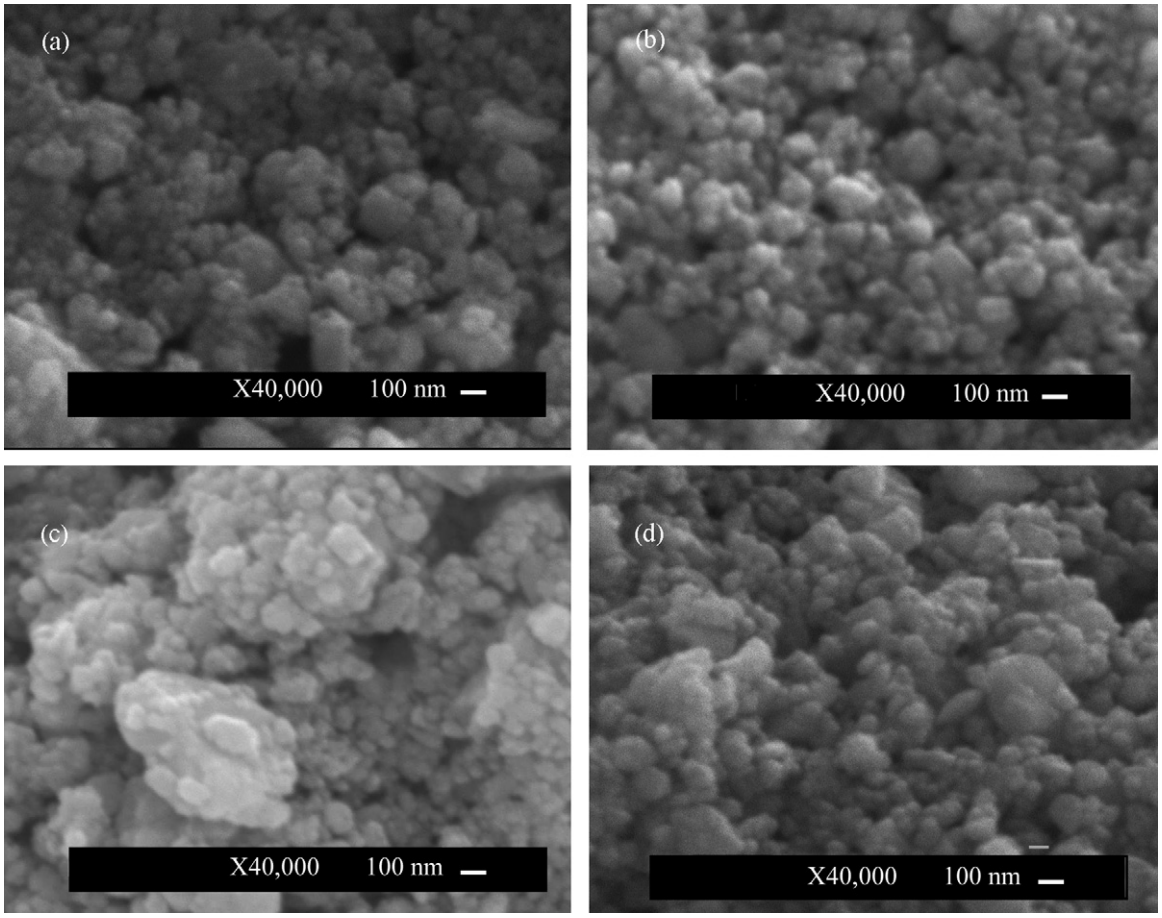

Fig. 5. SEM images of coated samples with higher magnification: (a) $La_{0.95}Ce_{0.05}CoO_3$, (b) $La_{0.9}Ce_{0.1}CoO_3$, (c) $La_{0.85}Ce_{0.15}CoO_3$ and (d) $La_{0.80}Ce_{0.2}CoO_3$.

ture was decreased slightly for all Ce-doped samples compared to that of the undoped one. Table 2 shows the amount of desorbed α-O_2 calculated by integrating the corresponding peaks for each sample. The total quantity of desorbed α-O_2 increased from 514 μmol/g for the undoped sample to 1259 μmol/g for 10 at% Ce-added sample. The amount of desorbed α-O_2 decreased substantially to 417 μmol/g by further addition of cerium. β-O_2 desorption, however, showed a monotonic behavior as a result of the cerium addition. The undoped sample exhibited a very small peak at 850 °C while it monotonically increased following the Ce addition.

According to the XRD patterns, the synthesized samples are the mixture of doped perovskite, and unreacted CeO_2 and Co_3O_4 while the mole fraction of the constituents varies according to the doping level. It is therefore difficult to decide which constituent is mainly responsible for the variations in α-O_2 and β-O_2 desorptions. In order to find out the possible effects of unreacted Ce and Co oxides on oxygen desorption profile, pure CeO_2 and Co_3O_4 samples were milled using the same procedure and subjecting them to the TPD-O_2 analysis. As shown in Fig. 3, the oxygen desorption of Co_3O_4 and CeO_2 started at 350 and 800 °C, respectively. The maximum height of Co_3O_4 was 20 times higher than that of CeO_2. These results suggest that the α-O_2 variation could not be attributed to the unreacted CeO_2 or Co_3O_4, since they do not desorb so much at this temperature range. The β-O_2 desorption could, however, be related to the presence of the unreacted Co_3O_4, since its desorption temperature corresponds to that of the pure Co_3O_4. By increasing the Ce addition level, the amount of unreacted Co_3O_4 increases leading to an increase in the β-O_2 desorption.

The TPD-O_2 results confirmed that cerium oxide alone does not desorb large amounts of oxygen at low temperature, but when added to the perovskite formulation, it promotes the α-O_2 desorption. This observation indirectly suggests that a part of Ce is introduced into the perovskite structure and modifies its oxygen mobility. The variation observed in the α-O_2 desorption as a function of Ce addition could therefore be explained by considering two competing phenomena. On the one hand, the addition of Ce keeps enhancing the α-O_2 of the perovskite until a saturation point is reached, after which no more Ce enters the perovskite structure. On the other hand, since CeO_2 does not react with Co_3O_4, further addition of Ce (at the expense of La) leads to an increase in the amounts of unreacted Co_3O_4 and CeO_2, and decreases the amount of the perovskite phase. Consequently, the amount of α-O_2 decreases due to the decrease in the amount of the perovskite phase. This is most likely the reason why the amount of α-O_2 increases with Ce addition and then decreases when the addition level exceeds a critical level. This critical level was found to be 10 at% Ce for the LaCeCo system.

SEM micrographs of the coated samples are shown in Fig. 4. These images show that the coating method was successful as

Table 2
α-O_2 results for synthesized samples.

Samples	α-O_2 (theoretical), μmol/g	α-O_2 (TPD-O_2), μmol/g	Ratio of α-O_2:TPD-O_2/theoretical
Ce0	264	514	1.94
Ce05	216	1076	4.98
Ce10	224	1259	5.62
Ce15	208	779	3.74
Ce20	200	417	2.08

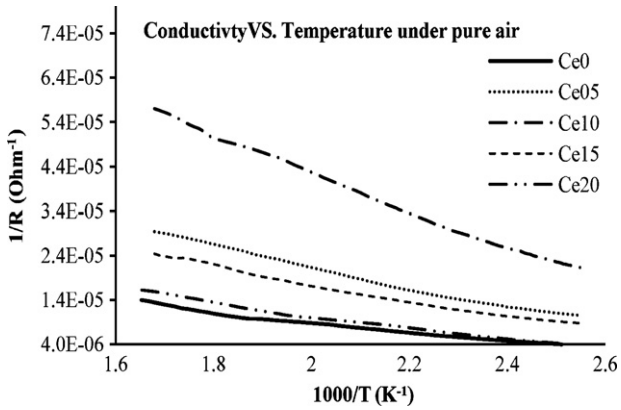

Fig. 6. Conductivity of coated samples as a function of temperature under pure air, Cex (x = mole fraction of doping in La-site fraction).

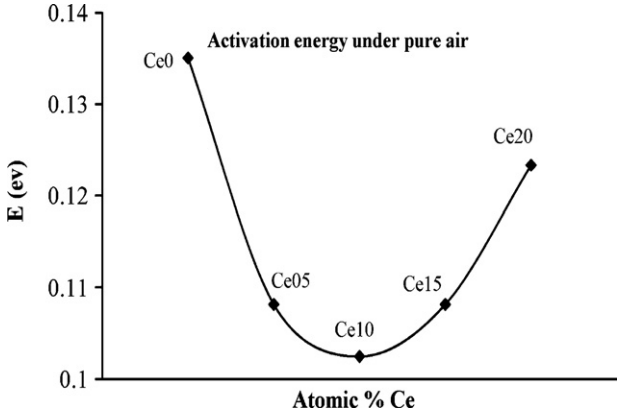

Fig. 7. Activation energy of coated samples under pure air, Cex (x = mole fraction of doping in La-site fraction).

a continuous and crack-free film on the alumina substrate was obtained. The morphology of the coated samples was, however, slightly different. By increasing the quantity of Ce, adhesion on the substrate improved and a smoother film was obtained. Higher magnifications showed quite similar degrees of agglomeration for all the samples (Fig. 5).

Fig. 6 shows the variation of conductivity as a function of temperature for the synthesized formulations in pure air at a temperature range of 100–300 °C. It can be seen that the conductivity of all the samples increased over the whole temperature range. However, the slope of the curves varies for different Ce addition levels.

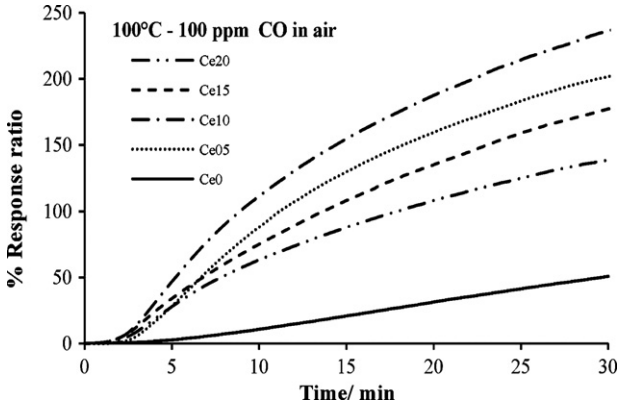

Fig. 8. Response ratio of coated samples under 100 ppm CO in air at 100 °C, Cex (x = mole fraction of doping in La-site fraction).

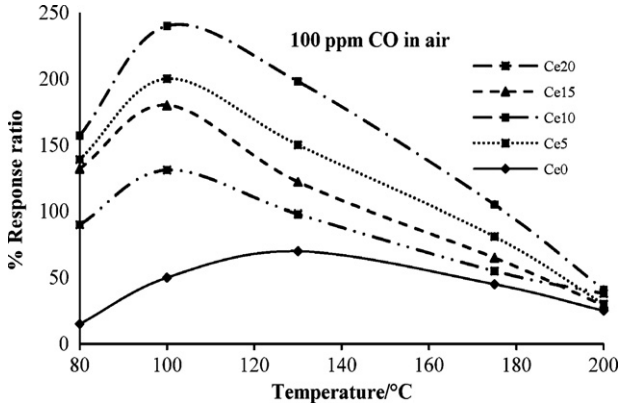

Fig. 9. Response ratio of coated samples vs. temperature, Cex (x = mole fraction of doping in La-site fraction).

The conductivity of the sensing films increased by Ce addition up to 10 at%, and decreased significantly by further increase in the Ce level. This variation is in perfect correlation with the α-O_2 desorption behavior of the samples as recorded by TPD-O_2. It seems that Ce addition increases the conductivity of the $LaCoO_3$ perovskite until the saturation point is attained. As discussed earlier, increasing Ce further (at the expense of La) would lead to an increase in the quantity of unreacted CeO_2 and of Co_3O_4 in the formulation. Since CeO_2 and Co_3O_4 are more resistant than perovskite, they decrease the overall conductivity of the sensing film.

The conductivity of all doped samples decreased by introducing CO into the testing atmosphere, confirming that the $La_{1-x}Ce_xCoO_3$ films behave as a p-type gas sensor, and that the conductivity should be governed by the hole density and mobility. The mobile holes are the electrical carriers in p-type semiconductors whose electrical conductivity can be expressed as [35]:

$$\sigma T = A \exp\left(\frac{-E_a}{kT}\right)$$

where σ stands for the conductivity, T for the absolute temperature (K), k for the Boltzmann constant, and E_a for the activation energy the charge carriers in the presence of pure air with $E_a = \Delta H_m + (E_g/2)$. ΔH_m is the motional enthalpy of holes and E_g is the band gap energy. Activation energy in the ambient air can be therefore obtained by plotting $\ln(\sigma T)$ as a function of $(1/T)$. Activation energy of all the samples were thus calculated and shown in Fig. 7. Again, the activation energy was found to be in perfect correlation with α-O_2 desorption behavior. It decreased first by increasing the Ce level reaching a minimum at 10 at% Ce addition and then decreased by further increase of Ce content.

The response ratios of doped materials with respect to the introduction of 100 ppm of CO into the testing atmosphere at 100 °C are shown in Fig. 8. The response ratio of all the doped formulations increased compared to that of the pure $LaCoO_3$. The optimum doping level of Ce was found to be 10 at% for this temperature, which resulted in a substantial increase in the response ratio by 5 times compared to that of the undoped perovskite.

In order to reveal the effect of temperature on gas testing properties and find the temperature of the maximum response ratio, all samples were tested in the presence of 100 ppm CO at different temperatures varying from 80 to 200 °C. The response ratios have been plotted as a function of temperature in Fig. 9. It can clearly be seen that Ce doping decreases the temperature of maximum response ratio from 130 °C for the pure $LaCoO_3$ to 100 °C for the doped samples. The variation of the maximum response ratio as a function of Ce doping level (Fig. 10) shows that the maximum response ratio also follows the same trend as that of the activation

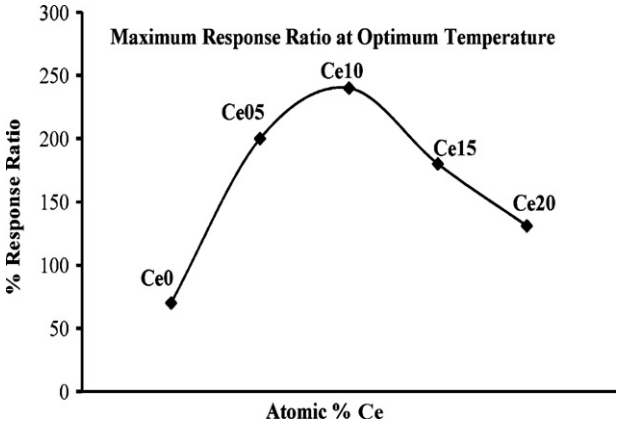

Fig. 10. Maximum response ratio of coated samples, Cex (x = mole fraction of doping in La-site fraction).

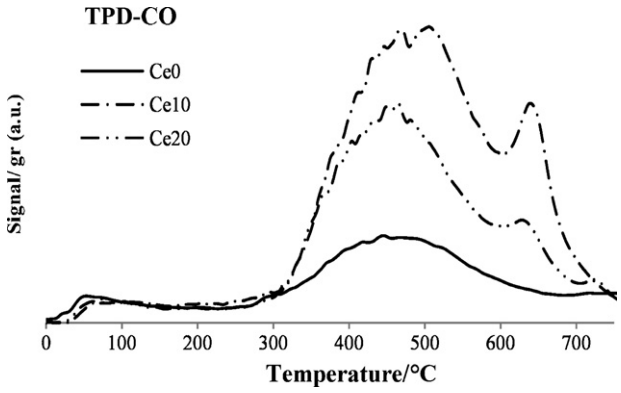

Fig. 11. XPS results showing binding energy of C 1s for Ce0 ($LaCoO_3$), Ce10 ($La_{0.9}Ce_{0.1}CoO_3$) and Ce20 ($La_{0.80}Ce_{0.2}CoO_3$) after two different gas-treatments: sample 300 °C-air: calcined at 300 °C under pure air; sample 100 °C-CO: calcined at 300 °C under pure air followed by cooling to 100 °C and be exposed to 100 ppm CO for 1 h and cooled to room temperature under the same atmosphere.

energy; i.e. a sharp increase following the Ce addition up to 10 at% and a decrease after further increase in the Ce level.

In our previous work [32], we reported the effect of processing parameters on gas testing performance, where a significant improvement in the response ratio was obtained for samples prepared by the activated reactive synthesis method. The improvement was attributed to the high specific surface area and large amounts of grain boundaries and, consequently, to the substantial increase in the α-O_2 desorption. The effect of α-O_2 on gas sensing properties was discussed using Rhee and Lee [36] observations that higher concentrations of surface oxygen could lead to a higher probability of finding two lattice oxygen ions with an appropriate distance, hence increasing the CO adsorption. The adsorption of CO and formation of stable monodentate carbonate on the surface may result in the creation of a stable depletion layer. CO adsorption on the lattice oxygen may also cause the migration of oxygen ions toward the particle surface through the grain boundaries, which results in the extension of the space charge layer inside the agglomerates. It was concluded that the oxygen mobility should play an important role in determining the sample response ratio.

Since the Ce doping showed a considerable influence on α-O_2 desorption, its effect on CO adsorption was also investigated. The CO storage capacity of the samples was therefore evaluated using temperature programmed desorption of CO. The samples were degreened at 300 °C and were subsequently cooled to 100 °C (similar to the XPS procedure). CO (100 ppm) was then injected into the atmosphere for 2 h before cooling the samples to room temperature under the same CO concentration. The samples were then put under the He flow and the temperature was increased at a rate of 5 °C/min. The outgoing gas was analyzed using a Fourier Transform Infra Red (FTIR) spectrometer. This procedure was chosen in order to simulate the gas sensing test procedure. Only CO_2, with no trace of CO, was detected in the outgoing gas. The CO_2 concentration has been plotted as a function of time in Fig. 11. Two major desorption peaks could be distinguished for Ce10 and Ce20 samples; the first one at the temperature range of 300–600 °C with the maximum at 475 °C, and the second at the range of 520–750 °C with the maximum at 620 °C. Different desorption temperature ranges indicate that the desorbed species have different bonding energies. The Ce20 sample exhibited a small additional peak at 730 °C. Considering a larger amount of unreacted Ce and Co oxides in this sample, this peak could be attributed to the decomposition of more stable Co or Ce carbonates.

Fig. 11 clearly shows the considerable effect of Ce doping on the CO storage capacity of the samples. The amounts of desorbed CO_2 calculated for each sample were 183, 562, and 376 μmol/g for undoped, Ce10 and Ce20 samples, respectively. Both CO_2 major desorption peaks follow the same trend as do the α-O_2 desorption curves presented in Fig. 2. This result strongly suggests that the α-O_2 on this type of perovskites is a dominant factor in the determination of the CO adsorption rate and of the CO storage capacity of the samples.

The surface composition of the samples was also examined using XPS. The samples were treated with the same procedure as that used for TPD-CO. The peaks related to C 1s species are shown in Fig. 12, and the normalized quantity of total carbon of each sample is presented in Table 3. Comparing the total surface carbon of the samples both before and after CO exposure reveals that the total amount of the surface carbon is relatively low for the undoped sample. For Ce10 sample, in contrast, the figure is at its highest, though showing a decreasing trend with further addition of Ce. This observation suggests that the Ce10 sample keeps the highest level of surface carbon even after degreening at 300 °C under pure air. Due to the CO exposure, the surface carbon of all samples increased but at different rates. The total amount of carbon increased by 0.4, 1.8 and 0.6 at% for undoped, C10 and C20 samples, respectively. These results are in agreement with the TPD-CO results presented in Fig. 11, and confirm that the CO adsorption increases by Ce addition while it decreases when Ce level exceeds 10 at%.

Deconvolution of the C 1s peaks resulted in three main photo lines at 285.6, 287.5 and 289.5 eV. The normalized quantity of each species is summarized in Table 3. C 1s photo line with lower (C_a), middle (C_b) and higher (C_c) energy are assigned to the monodentate carbonate, carbonyl and bidentate carbonate groups, respectively [36]. It has been reported that in the carbonyl group, carbon can bond to Co^{3+} by electron back-donation, but that in the carbonate groups (monodentate or bidentate), CO bonds to the lattice oxygen [36]. Bonding the CO to Co decreases the conductivity due to the donor dopant effect on the surface, and bonding to O^{2-} releases

Table 3
Quantitative amounts of different C 1s carbon species obtained by deconvolution of C 1s spectra of Fig. 11.

Sample	Treatment condition	%Atomic concentrations			
		C_a	C_b	C_c	Total C
Ce0	300 °C-under pure air	0.4	0.2	0.5	1.1
	100 °C-under 100 ppm CO	0.6	0.2	0.7	1.5
Ce10	300 °C-under pure air	0.3	0.2	3.3	3.8
	100 °C-under 100 ppm CO	1.4	0.3	3.9	5.6
Ce20	300 °C-under pure air	0.3	0.4	2.6	3.3
	100 °C-under 100 ppm CO	0.8	0.4	2.7	3.9

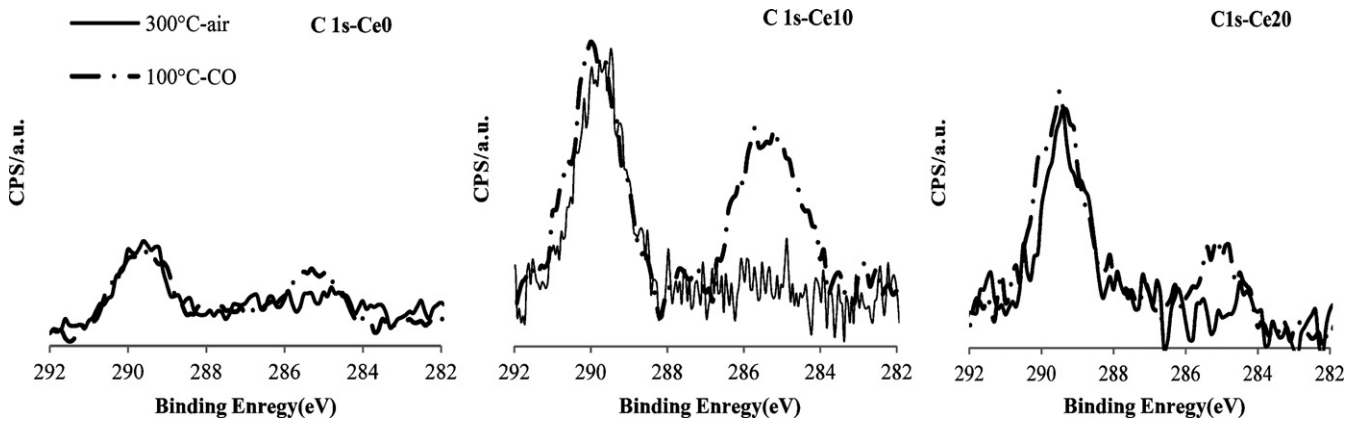

Fig. 12. TPD-CO spectra of Ce0 ($LaCoO_3$), Ce10 ($La_{0.9}Ce_{0.1}CoO_3$) and Ce20 ($La_{0.80}Ce_{0.2}CoO_3$).

electron which has the same effect on the conductivity. By introducing CO, the peak related to carbonyl (C_b) remains almost unchanged while the peaks related to C_a and C_c increase. The variation in C_a carbon is higher than that in the C_c carbon for both samples. The highest variation is related to the monodentate carbon (C_a), with a 1.1% increase for the Ce10 sample. Although the amounts of both C_a and C_c species follow the same trend as that of the total carbon, the C_a carbon is systematically higher than C_c for the Ce-doped samples suggesting that CO preferentially adsorbs on the lattice oxygen. These results are in agreement with the hypothesis which assumes the adsorption of CO on two neighbouring lattice oxygen ions followed by the formation of stable monodentate carbonate.

Fig. 13 shows the dependence of the response ratio of our best sample (Ce10) to CO concentration in the range of 20–500 ppm at 100 °C. The change in resistivity as a function of CO concentration can be expressed as:

$$R \approx AC_{CO}^{\alpha}$$

where R is the resistance of Ce10, C_{CO} is the concentration of CO in air, and A and α are constants. Higher values of α signifies higher sensitivity of the sensor to gas concentration. In SnO_2-based sensors, α lies in the range of 1/6 to 1/2 [37,38]. When the resistance of Ce10 was sent, α was found to be 0.6 for Ce10 in the range of 20–500 ppm of CO in air.

To sum up, the results of the experiments clearly showed that Ce has a significant effect on the α-O_2 desorption of LaCo-based perovskites, with the maximum occurring at 10 at% addition level. α-O_2, in turn, influences the conductivity, activation energy, CO adsorption, and response ratio of the material. All these properties follow the same trend showing an optimum at 10 at% Ce addition level. Considering the structural evolution of the samples as well as the α-O_2 desorption of pure CeO_2 and Co_3O_4, the behavior of these materials cannot be attributed to the simple mixing of CeO_2 with perovskite since otherwise the α-O_2 desorption would increase monotonically following Ce addition. This suggests that Ce^{4+} to some extent enters the perovskite structure and affects its electronic and ionic behavior. In such a case, in order to achieve an electro-neutrality state in the structure of $La_{1-x}Ce_xCoO_3$, Co^{3+} should change into Co^{2+} and/or the structure should contain extra oxygen. Based on the broadening of XRD peaks, Forni et al. [33] concluded that Ce substitutes in the LaCo-based perovskite structure. The solubility limit of Ce in $La_{1-x}Ce_xCoO_3$ structure, however, prevents unlimited substitution of Ce in the perovskite structure and a saturation point is reached. A saturation point of 5–10 at% Ce has been reported in the literature [33]. The samples synthesized using activated reactive synthesis exhibit additional broadening of XRD peaks due to the internal stress and crystallite size effect. In this way, the results did not allow for the confirmation of Ce substitution in the perovskite structure. However, the results of parallel characterizations suggest that Ce enters the perovskite structure although it is not possible to determine its exact substitution level. The effect of Ce addition is thus accounted for by two phenomena that simultaneously influence the sensing behavior of these materials. First, Ce substitutes for La, thereby increasing the α-O_2, and consequently the conductivity, CO adsorption rate and response ratio, and low intrinsic activation energy. Further addition of Ce, at the expense of La, will result in a saturation point while unreacted precursors (CeO_2 and Co_3O_4) appear and the total amount of perovskite is reduced. The unreacted precursors with a low α-O_2 desorption, higher resistivity, and no response to CO decrease the overall conductivity, CO adsorption and response ratio.

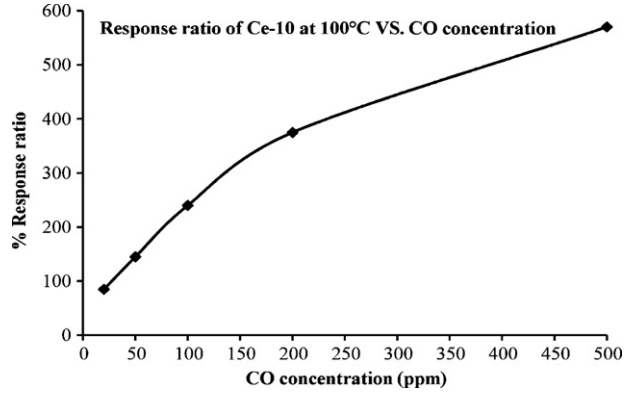

Fig. 13. Maximum response ratio of Ce10 ($La_{0.9}Ce_{0.1}CoO_3$) sample at different CO concentrations.

4. Conclusion

Nanostructured $La_{1-x}Ce_xCoO_3$ ($0 \le x \le 0.2$) with a crystallite size of 12–13 nm and a high specific surface area of 55 m^2/g were prepared using activated reactive synthesis method. TPD-O_2 results revealed that cerium provides more α-oxygen on the surface which bonds to the adsorbed CO and increases the response ratio of the sensing layer. The amount of α-O_2 was found to be the most significant parameter influencing the sensing properties of this type of perovskite. This oxygen is the weakly bonded oxygen which is desorbed at a temperature range between 300 and 650 °C. The physico-chemical properties of the sensing layer such as conductivity, activation energy, maximum CO adsorption and maximum response ratio of the sensing materials were found to be influenced by the amount of α-O_2. XRD results of the samples with different

Ce doping levels showed that there is a limitation on cerium doping in the perovskite structure. Extra cerium could no longer enter the structure when the cerium content is increased which results in the formation of unreacted Ce and Co oxides. Increasing unreacted materials caused the negative effect of cobalt oxide to overshadow the positive effect of cerium doping, allowing for the observation of the optimum overall effect on the samples' sensing properties. The optimum amount of Ce doping was found to be 10 at% where a maximum value was obtained for α-oxygen desorption, conductivity, response ratio, and CO adsorption. Partial substitution of 10 at% of Ce on La site showed an approximately four-time increase in the response ratio (240%) with respect to 100 ppm CO at 100 °C. The sample with an optimum Ce level showed a good sensitivity with respect to CO presenting a response ratio of 90% for 20 ppm CO at 100 °C.

Acknowledgement

The authors wish to acknowledge the Natural Sciences and Engineering Council of Canada for financial support of this work.

References

[1] M.A. Pena, J.L.G. Fierro, Chemical structures and performance of perovskite oxides, Chem. Rev. 101 (2001) 1981–2017.
[2] S. Arakawa, H. Kurachi, J. Shiokawa, Physicochemical properties of rare earth perovskite oxides used as gas sensor material, J. Mater. Sci. 20 (2005) 1207–1210.
[3] Z.G. Zhou, Z.L. Tang, Z.T. Zhang, W. Wlodarski, Perovskite oxide of PTCR ceramics as chemical sensors, Sens. Actuat. B: Chem. 77 (2001) 22–26.
[4] M.L. Post, J.J. Tunney, D. Yang, X. Du, D.L. Singleton, Material chemistry of perovskite compounds as chemical sensors, Sens. Actuat. B: Chem. 59 (1999) 190–194.
[5] L.G. Tejuca, Properties and Applications of Perovskite-type Oxides Chemical Industries, CRC Press, Madrid, 1993.
[6] J.W. Fergus, Perovskite oxides for semiconductor-based gas sensors, Sens. Actuat. B: Chem. 123 (2007) 1169–1179.
[7] Z. Zhou, Z. Tang, Z. Zhang, Studies on grain-boundary chemistry of perovskite ceramics as CO gas sensors, Sens. Actuat. B: Chem. 93 (2003) 356–361.
[8] N.N. Toan, S. Saukko, V. Lantto, Gas sensing with semiconducting perovskite oxide $LaFeO_3$, Phys. B 327 (2003) 279–282.
[9] A.V. Salker, N.J. Choi, J.H. Kwak, B.S. Joo, D.D. Lee, Thick films of In, Bi and Pd metal oxides impregnated in $LaCoO_3$ perovskite as carbon monoxide sensor, Sens. Actuat. B: Chem. 106 (2005) 461–467.
[10] R. Zhang, A. Villanueva, H. Alamdari, S. Kaliaguine, Reduction of NO by CO over nanoscale $LaCo_{1-x}Cu_xO_3$ and $LaMn_{1-x}Cu_xO_3$ perovskites, J. Mol. Catal. A: Chem. 258 (2006) 22–34.
[11] C.M. Chiu, Y.H. Chang, The influence of microstructure and deposition methods on CO gas sensing properties of $La_{0.8}Sr_{0.2}Co_{1-x}Ni_xO_{3-\delta}$ perovskite film, Sens. Actuat. B: Chem. 54 (1999) 236–242.
[12] L. Zhang, J. Hu, P. Song, H. Qin, K. An, X. Wang, M. Jiang, CO-sensing properties of perovskite $La_{0.68}Pb_{0.32}FeO_3$ nano-materials, Sens. Actuat. B: Chem. 119 (2006) 315–318.
[13] P. Song, H. Qin, X. Liu, S. Huang, R. Zhang, J. Hu, M. Jiang, Structure, electrical and CO-sensing properties of the $La_{0.8}Pb_{0.2}Fe_{1-x}Co_xO_3$ system, Sens. Actuat. B: Chem. 119 (2006) 415–418.
[14] V. Lantto, S. Saukko, N.N. Toan, L.F. Reyes, C.G. Granqvist, Gas sensing with perovskite-like oxides having ABO_3 and BO_3 structures, J. Electroceram. 13 (2004) 721–726.
[15] Y.L. Chai, D.T. Ray, H.S. Liu, C.F. Dai, Y.H. Chang, Characteristics of $La_{0.8}Sr_{0.2}Co_{1-x}Cu_xO_{3-\delta}$ film and its sensing properties for CO gas, Mater. Sci. Eng. A A293 (2000) 39–45.
[16] G. Cairong, F. Guoliang, H. Yanfeng, S. Chonglin, H. Qifei, Z. Zhongrong, Properties of $La_{1-x}Ce_xCoO_3$ system perovskite-type catalysts for diesel engine exhaust removal, Front. Chem. Eng. China 1 (2007) 6–10.
[17] E. Campagnoli, A.C. Tavares, L. Fabbrini, I. Rossetti, Yu.A. Dubitsky, A. Zaopo, L. Forni, $La_{1-x}A_xCo_{1-y}Fe_yO_3$ (A = Ce, Sr) catalysts for the flameless combustion of methane, J. Mater. Sci. 41 (2006) 4713–4719.
[18] T. Nitadori, M. Misono, Catalytic properties of $La_{1-x}A_xFeO_3$ (A = Sr, Ce) and $La_{1-x}Ce_xCoO_3$, J. Catal. 93 (1985) 459–466.
[19] N.E. Machin, C. Karakaya, A. Celepci, Catalytic combustion of methane on La-, Ce-, and Co-based mixed oxides, Energy Fuel 22 (2008) 2166–2171.
[20] Y. Wen, C. Zhang, H. He, Y. Yu, Y. Teraok, Catalytic oxidation of nitrogen monoxide over $La_{1-x}Ce_xCoO_3$ perovskites, Catal. Today 126 (2007) 400–405.
[21] K. Tabata, I. Matumoto, Catalytic properties and surface states of $La_{1-x}Ce_xCoO_3$, J. Mater. Sci. 22 (1987) 4031–4035.
[22] G. Williams, G.S.V. Coles, Gas sensing properties of nanocrystalline metal oxide powders produced by a laser evaporation technique, J. Mater. Chem. 8 (1998) 1657–1664.
[23] W. Zhou, Z. Shao, W. Jin, Synthesis of nanocrystalline conducting composite oxides based on a non-ion selective combined complexing process for functional applications, J. Alloys Compd. 426 (2006) 368–374.
[24] H. Shimooka, M. Kuwabara, Crystallinity and stoichiometry of nano-structured sol–gel-derived $BaTiO_3$ monolithic gels, J. Am. Chem. Soc. 79 (1996) 2983–2985.
[25] S. Zhaoa, J.K.O. Sina, B. Xub, M. Zhaob, Z. Pengb, H. Caib, A high performance ethanol sensor based on field-effect transistor using a $LaFeO_3$ nano-crystalline thin-film as a gate electrode, Sens. Actuat. B: Chem. 64 (2000) 83–87.
[26] S.H. Lee, J.Y. Lee, Y.M. Park, J.H. Wee, K.Y. Lee, Complete oxidation of methane and CO at low temperature over $LaCoO_3$ prepared by spray-freezing/freeze-drying method, Catal. Today 117 (2006) 376–381.
[27] A. Worayingyong, P. Kangvansura, S. Kityakarn, Schiff base complex sol–gel method for $LaCoO_3$ perovskite preparation with high-adsorbed oxygen, Colloid Surf. A 320 (2008) 123–129.
[28] H. Alamdari, S. Boily, M. Blouin, A. Van Neste, R. Schulz, High energy ball milled nanocrystalline ZnO varistors, Mater. Sci. Forum 343–346 (2000) 909–917.
[29] S. Kaliaguine, A. Van Neste, V. Szabo, E.J. Gallot, M. Bassir, R. Muzychuk, Perovskite-type oxides synthesized by reactive grinding. Part I. Preparation and characterization, Appl. Catal. A: Gen. 209 (2001) 345–358.
[30] S. Royer, H. Alamdari, D. Duprez, S. Kaliaguine, Oxygen storage capacity of $La_{1-x}A'_xBO_3$ perovskites (with A′ = Sr, Ce; B = Co, Mn)—relation with catalytic activity in the CH_4 oxidation reaction, Appl. Catal. B: Environ. 58 (2005) 273–288.
[31] S. Royer, D. Duprez, S. Kaliaguine, Role of bulk and grain boundary oxygen mobility in the catalytic oxidation activity of $LaCo_{1-x}Fe_xO_3$, J. Catal. 234 (2005) 364–375.
[32] M. Ghasdi, H.D. Alamdari, CO sensitive nanocrystalline $LaCoO_3$ perovskite sensor prepared by high energy ball milling, Sens. Actuat. B: Chem. 148 (2010) 478–485.
[33] L. Forni, C. Oliva, T. Barzetti, E. Selli, A.M. Ezerets, A.V. Vishniakov, FT-IR and EPR spectroscopic analysis of $La_{1-x}Ce_xCoO_3$ perovskite-like catalysts for NO reduction by CO, Appl. Catal. B: Environ. 13 (1997) 35–43.
[34] R. Leanza, I. Rossetti, L. Fabbrini, C. Oliva, L. Forni, Perovskite catalysts for the catalytic flameless combustion of methane: preparation by flame-hydrolysis and characterisation by TPD-TPR-MS and EPR, Appl. Catal. B: Environ. 28 (2000) 55–64.
[35] M.A. Senaris-Rodriguez, J.B. Goodenough, $LaCoO_3$ revisited, J. Sol. State Chem. 116 (1995) 224–231.
[36] C.K. Rhee, H. Lee, Co oxidation on $LaCoO_3$ perovskite, Korean J. Chem. Eng. 11 (1994) 48–54.
[37] P.K. Clifford, D.T. Tuma, Characteristics of semiconductor gas sensors. I. Steady state gas response, Sens. Actuat. 3 (1982) 233–254.
[38] J. Watson, K. Ihokura, G.S.V. Coles, The tin dioxide gas sensor, Meas. Sci. Technol. 4 (1993) 711–719.

Biographies

Mohammad Ghasdi received his BSc degree in Chemical Engineering (2004) from Tehran University, and MSc degree in Transport Phenomena (2007), Chemical Engineering, from Sharif University of Technology. He is currently studying for a PhD degree at the Department of Mining, Metallurgical and Materials Engineering, Université Laval. His current research interests include synthesis, characterization and fabrication of nanomaterials for metal oxide gas sensor applications.

Houshang Alamdari received MSc degree in 1996 and PhD degree in 2000 from Université Laval, Canada. He pursued his research activities at Hydro-Québec Research Institute, Canada on synthesis of nanocrystalline materials for hydrogen storage. He held the process director position at Nanox Inc., Canada and was involved in development and scale up of a production process for nanostructured perovskite-type materials for automotive catalysts. He is currently a professor at the Department of Mining, Metallurgical and Materials Engineering, Université Laval, Canada.

Sébastien Royer received his master degree in 2001 from the University Pierre et Marie Curie/ENSPM. He pursued his academic formation at Université Laval, Canada, where he obtained a PhD in Chemical Engineering in 2004. After one year postdoctoral stay at the French Petroleum Institute, he got a position of Associated Professor at LACCO, University of Poitiers, France. His current research is focusing on the design of size- and pore-controlled active oxides for applications in environment and energy.

Alain Adnot received his BSc in physical engineering from Institut National des Sciences Appliquées, Lyon (France), MSc and PhD degrees in physics from Université Laval, Canada in 1972 and 1977, respectively. He was working as development engineer in surface analysis instrumentations at Rueil (France) until 1981, and as research scientist at Institut des Matériaux Industriel, Boucherville, Canada until 1983. Since 1983 he is responsible for the surface analysis laboratory at Laval University, Canada.